Visual Abstract

Fatigue crack growth analysis of welded bridge details

Danilo D'Angela
University of Naples Federico II, Italy
danilo.dangela@unina.it, http://orcid.org/0000-0002-8096-5202

Marianna Ercolino
University of Greenwich, UK
m.ercolino@gre.ac.uk, http://orcid.org/0000-0001-8678-0631

ABSTRACT. The paper investigates the fatigue crack growth in typical bridge weldments by means of numerical analysis. The extended finite element (XFEM) method is coupled with the low-cycle fatigue (LCF) approach in ABAQUS, and parametric analyses are carried out in order to assess the influence of the main sample/testing features on the fatigue life of the investigated structures. The numerical results are found to be robust and reliable by performing comparisons with past experimental data and regulation design correlations.

KEYWORDS. Crack growth; Fatigue; Welded details; XFEM; ABAQUS.

OPEN ACCESS

Citation: D'Angela, D., Ercolino, M., Fatigue crack growth analysis of welded bridge details, Frattura ed Integrità Strutturale, 60 (2022) 265-272.

Received: 03.02.2022
Accepted: 07.02.2022
Online first: 08.02.2022
Published: 01.04.2022

INTRODUCTION

Fatigue crack propagation is among the most critical damage mechanisms affecting metallic structures and infrastructures subjected to repeated loading [1–4]. Welded details are typically extremely sensitive to crack propagation phenomena. The welding process can generate flaws and defects in the vicinity of the weldment toe, and such pre-cracks can easily activate crack development [5] especially if the applied load is orthogonal to the crack surface (e.g., *mode I* fracture).

Numerical simulation by means of finite element (FE) analysis is among the most reliable tools for the assessment of the fatigue crack propagation in metallic structures and for the estimation of their fatigue life [6–10]. The extended finite element method (XFEM) is among the most advanced technologies for simulating fracture phenomena, and several recent studies proved that it could be reliable also regarding fatigue crack propagation in metals [1,11–16]. Hedayati and Vajedi [15] developed robust modelling of crack propagation in slant cracked plates based and provided estimations of the fatigue life. Melson [17] analysed the fatigue response of aluminium crack plates and found that XFEM technology can be more reliable than other methodologies. Other authors [7,8] implemented subroutines for more accurate simulations, and they found reliable results. In spite of the available methodologies and the copious literature, there are still several issues affecting the FE analysis of fatigue and fracture phenomena, and novel approaches are needed to enhance the numerical analysis of fatigue crack propagation in metallic structures. The available models are often extremely complex and not suitable for practitioners, and the modelling parameters are not often physical based. In many cases, the analyses require high computational costs and the numerical results have been validated only considering theoretical or analytical data. In order to cover this gap, a simple but reliable numerical model is presented in this study. The XFEM technology is coupled with low-cycle fatigue (LCF) approach and parametric analyses are performed in ABAQUS [18]. The case study consists of welded bridge details, which are critical systems undergoing fatigue crack propagation and are less studied in the literature.

NUMERICAL MODELLING AND FATIGUE ANALYSIS

A three-dimensional model was built in ABAQUS coupling XFEM and LCF approach. In particular, the modelling was based on an improvement and extension of a pilot model developed by the authors considering bi-dimensional metallic plates [9,13]. The reference geometry, along with the initial crack, is shown in Figure 1a. S355 steel was assumed as a material. The structures consisted of (a) main plate, (b) gusset plate, and (c) main-to-gusset plate welded connection (Figure 1a). The main model had geometry dimensions W, L, δW, and δL equal to 60, 50, 10, and 8 mm, respectively; the initial crack length dimensions a and b were equal to 2 and 4 mm, respectively (Figure 1a).
All surface connections between the parts were assumed to be perfectly tied. The initial plane pre-crack surface (a x b) was assigned to the model (main plate) according to the most common location and size of flaws/defects in welded details, i.e., at the toe of the weldment and orthogonally to the direction of the typically applied stress [5]. In particular, the main plate is assumed to carry the most significant load, which is applied along with the longitudinal direction of the latter. Therefore, the pre-crack (weldment defect) is perpendicular to the direction of the applied load, and it can develop and activate the crack propagation phenomena.
Linear elastic homogeneous behaviour was assigned to the material according to the LEFM approach. The fracture response was implemented on the initial XFEM crack, according to Paris law (*fatigue fracture criterion* and *surface behavior*). The *mixed-mode power law* was used as a default ABAQUS model. The fatigue properties and the modelling parameters assumed for S355 steel are shown in Table 1, which were derived from the literature [19–21]. The boundary and loading conditions are shown in Figure 1.b. The stump cross sections of both main and gusset plates were fixed to simulate a symmetry condition. The cyclic loading P was applied to the reference middle section point, which was coupled to the whole surface by using a *continuum distribution* node-surface interaction. A cyclic frequency equal to 10 Hz was used, with a linear shape.

Material	Fatigue properties (mechanical)			Modelling parameters (ABAQUS code)		
	c_p	m_p	K_C	c_3	c_4	G_C
	$\left[\frac{\text{m}}{\text{cycle}\left(\text{MPa m}^{0.5}\right)^{\text{mp}}}\right]$	[-]	$\left[\text{MPa m}^{0.5}\right]$	$\left[\frac{\text{m / cycles}}{(\text{N / m})^{c_4}}\right]$	[-]	$\left[\frac{\text{kN}}{\text{m}}\right]$
S355 steel	5.71E−13	3.56	45	3.54E−14	1.781	9.6
7 % nickel steel	2.17E−11	2.57	135	2.80E−12	1.285	90.0
7075-T6 aluminium alloy	3.33E−11	3.70	25	2.55E−13	1.850	9.0

Table 1: Fatigue properties of the investigated materials and model parameters.

The numerical analysis consisted of two steps: *general static* and *direct cyclic* (LCF). The static analysis step was only performed to improve the convergence of the analysis, as it was previously found by pilot studies [9], as well as reported in the literature [22]. The static step included only one cycle, with negligible values of the applied force (no influence on the actual fatigue response). Several force values were applied to cover a wide range of applied stresses, i.e., from 75 to 325 MPa. This was aimed at evaluating the *S-N* curve, typically considered for the assessment of this typology of structures [5].
The model parts were partitioned (Figure 1c) to control the mesh size along with the distance from the FPZ. Only hexahedral elements (*8-node linear brick elements*) can be used in ABAQUS for three-dimensional modelling according to LCF-XFEM analysis, i.e., *C3D8* (full integration) and *C3D8R* (reduced integration) elements [18]. The reduced integration elements are typically more used in the literature (than the full integration ones) since they were found to be accurate for

modelling crack propagation problems despite the gain in smaller computational costs [9,15,23]. Therefore, the mesh size analysis was performed considering this type of mesh. The mesh size of the model was assigned in the light of an expeditious convergence analysis. The mesh sizes are depicted in Figure 1c, where the sizes related to part A, B, C, and D were equal to 0.7 x 0.7 mm, 0.7 x 4.5 mm, 4.0 x 4.0 mm, and 4.5 x 4.5 mm.

PARAMETRIC ANALYSIS

The influence of several sample features was assessed considering the main model as a reference (defined as model *m*). Material, structure geometry, and initial crack dimension/shape were varied, defining six parametric models. 7075-T6 aluminium alloy and 7% nickel steel were considered as alternative materials for generating models *M1* and *M2*. The related properties and modelling/analysis features are reported in Table 2. Two alternative structure geometries were considered, defining models *G1* and *G2*, together with the main model geometry. In particular, the models have geometry *W*, *L*, *dW*, and *dL* equal to (*G1*) *120*, 50, 10, and 8 mm, and (*G2*) *60*, 50, 20, and 8 mm. Two alternative pre-crack dimensions were considered; the related models are defined *C1* and *C2*; the models have dimensions *a* and *b* equal to (*C1*) 2 and *2* mm, and (*C2*) 2 and *8* mm. Constant-amplitude analyses were performed for all models from applied stress equal to 75 MPa up to 350 MPa, considering increments of 25 MPa. Overall, 72 analyses were performed.

(a) (b)

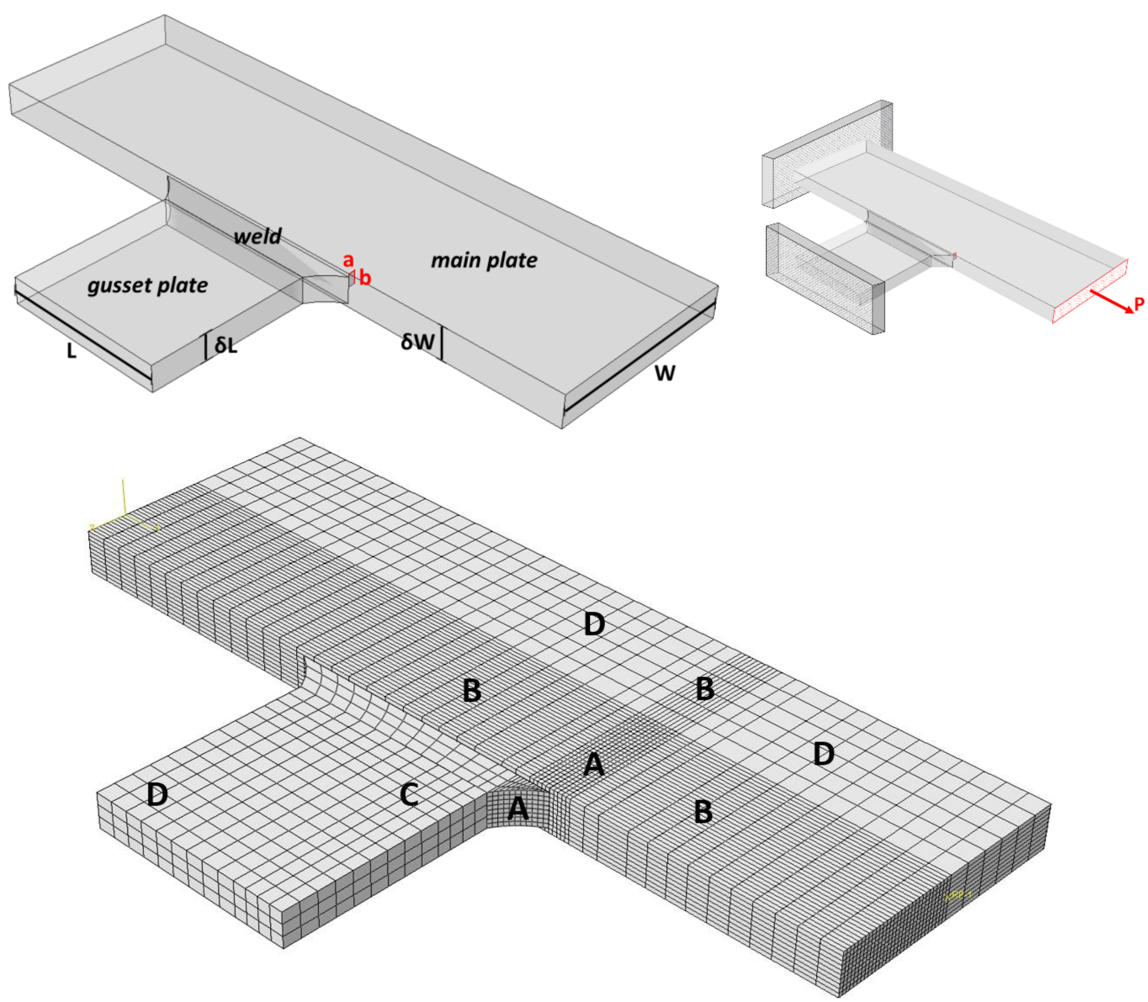

(c)

Figure 1: (a) Geometry of the welded detail (W, L, δW, and δL) with initial pre-crack dimensions, (b) schematic of the boundary and loading conditions, and (c) mesh partitions and sizes resulting from the convergence analysis.

RESULTS AND DISCUSSION

Fig. 2 shows the comparison between the numerical and the experimental results [5], where the nominal stress approach was considered. Data having N_f lower than 1×10^3 cycles were not considered. The numerical results over 2.785×10^4 to 2.54012×10^6 cycles (e.g., ~75 to ~250 MPa) were fitted with very good accuracy (e.g., $r^2 > 0.995$) using power law. This range of cycles is consistent with the typical values related to fatigue loading of such types of structures [5].The best-fit constants a_m and β_m were equal to 5.297×10^3 and -0.286, respectively. The experimental results are related to a large number (487) of fatigue tests on similar structures having the geometrical parameters W, L, δW, and δL ranging within 40 ÷ 170 mm, 50 ÷ 400 mm, 8 ÷ 20 mm, and 8 ÷ 20 mm, respectively. In Figure 2, the Eurocode 3 *S-N* (nominal stress approach) related to the investigated detail is also shown (nominal stress approach), i.e., C40 detail class curve [5,24]. The numerical results match with a good agreement the cloud of the experimental data, being on the safe side if the C40 class detail curve is considered. It is recalled that the experimental results are representative of an extremely wide range of geometries; furthermore, the numerical modelling considered a pre-crack with a definite geometry. Even though the validation of the model should be performed comparing cases having the same geometry/loading conditions, the numerical modelling is confirmed to be a reliable assessment of the fatigue life of complex welded details. This is supported by the log-log linear S-N correlation over the relevant stress-cycle ranges and by the location of the numerical data over the cloud of experimental results. As already mentioned, the model should be properly validated by considering specific case studies, e.g., as it was done with regard to the CT specimens.

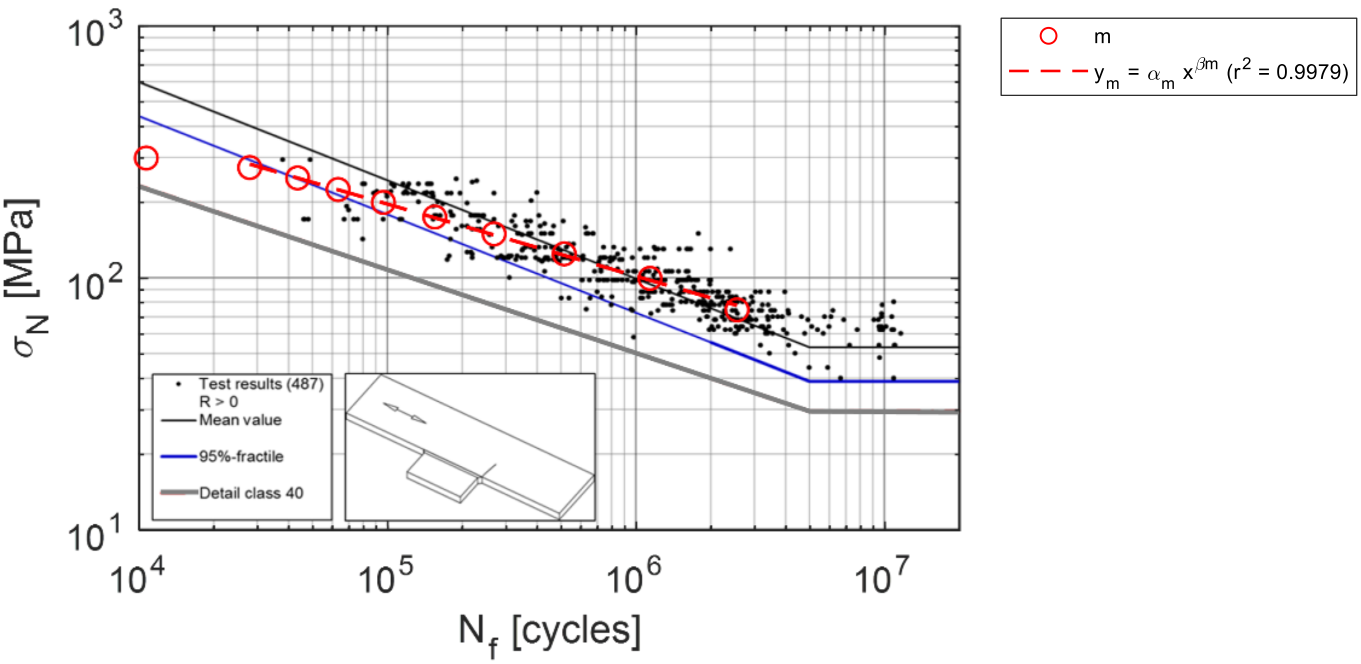

Figure 2: Comparison between the numerical results (red circles and red dashed line) and the experimental results (black dots and thin black and blu lines) reported by Aygül et al. [5] and Aygül [25], together with the C40 detail class curve (thick grey line) provided by Eurocode 3 [5,24].

The influence of the parametric variables was assessed by considering the *S-N* curves and both the parameters and the domain stress-cycle ranges related to the best-fit power laws. Figure 3 shows the results considering the variation of (a) the material (models *M1* and *M2*), (b) the structural geometry (models *G1* and *G2*), and (c) the pre-crack shape/dimension (models *C1* and *C2*). The best-fit power laws (with related r^2) are also shown. In particular, the data were fitted over the largest cycle interval that is associated with a power law having r^2 larger than 0.950. The values of the related best-fit constants and the corresponding cycle ranges are given in Figure 3. "EL" in (b) represents the endurance limit, i.e., the fatigue life was larger than 10^8 cycles for stresses lower than the represented case.

Model ID	α	β	r^2	range of fitting	
				from	to
	[-] / 10^3	[-]	[-]	[cycles] / 10^3	[cycles] / 10^5
<u>*m*</u>	5.2971	-0.286	0.9979	27.85	25.4012
M1	1.9953	-0.252	0.9636	1.25	3.7826
M2	26.5302	-0.452	0.9991	16.36	4.0925
G1	8.1892	-0.329	0.9993	22.58	14.6633
G2	1.3941	-0.149	0.9592	71.43	69.6150
C1	6.0073	-0.305	0.9826	8.82	14.7419
C2	3.8580	-0.265	0.9815	9.73	21.2300

Table 2: Values of the best-fit constants defined in Figure 3.

The material clearly affects the fatigue performance as well as the range in which the S-N data are stable (e.g., log-log linear). Model *M1* shows a lower best-fit efficiency if compared to other cases. The geometry related to the double width of the main plate (*M1*) has S-N data (slightly) less performing than the main model, especially for larger numbers of cycles (e.g., larger than 10^5). It is recalled that all models have the same nominal applied stress; therefore, models *G1* and *G2* have a double total applied force with respect to the main model. If the main plate has a double thickness (i.e., model *G2*), the performance significantly improves, especially for larger numbers of cycles (e.g., larger than 10^5). For a low number of cycles, *G2* has a performance comparable to the reference model m. The endurance limit (EL) is reached in model *G2* corresponding to stresses lower than 125 MPa (not observed in other cases over the same stress range). Best-fit efficiency related to model *G2* is reduced if compared to other cases, even though fewer data points were best-fitted.

The size of the initial crack does not significantly affect the performance of the components. However, very interesting results are observed if model *C1* is compared to the reference model m. *C1* presents a (slightly) lower performance even though one of the dimensions of the initial crack is half the main model one. In particular, model *C1* has the same crack dimensions *a* and *b* (equal 2 mm), whereas model m has the same *C1* dimension for *a* and double for *b*. This confirms that the shape of the initial crack (e.g., a/b) is more significant than the area ($a \cdot b$) for the determination of the fatigue performance of the component. A similar result can be observed with regard to model *C2*, where *b* is equal to four times *a*. In fact, the fatigue performance is quite similar to model m (*C1*) for a higher (lower) number of cycles. This confirms that a component having an initial crack with a shape ratio (a/b) equal to 1/2 is (slightly) more critical than elements having larger or smaller ratios. Obviously, this trend is related to the specific application and the investigated conditions. The provided values of the best-fit parameters allow quantifying the differences in fatigue life estimations among the different models, and they allow assessing the fatigue performance of similar components by producing a quick estimation.

Figure 4 shows the comparison between the numerical results (best-fit) related to (a) models *m*, *G1*, and *G2* and (b) models *m*, *C1*, and *C2* and the data related to the experimental database previously considered to assess the main model results [5,25]. Such models are compatible with the geometrical properties of the considered experimental database. The curve related to the detail class C40 is also shown [5,24]. It is recalled that the cloud of experimental data is related to a wide range of geometries, i.e., *W*, *L*, δW, and δL ranging within 40 ÷ 170 mm, 50 ÷ 400 mm, 8 ÷ 20 mm, and 8 ÷ 20 mm, respectively. However, the variation of the modelling geometry (*W* equal to 60 and 120 mm, and δW equal to 10 and 20 mm) approximately envelope the cloud of experimental data. In particular, the superior enveloping related to model *G2* is qualitatively consistent with the fact that this case is associated with δW equal to 20 mm, which corresponds to the maximum value over the experimental case. Similarly, model *G1*, which is corresponding to W equal to 120 mm, shows results in the inferior part of the experimental cloud, which has maximum W equal to 170 mm. Such qualitative trends strengthen the robustness of the modelling approach, even though proper validation should be performed.

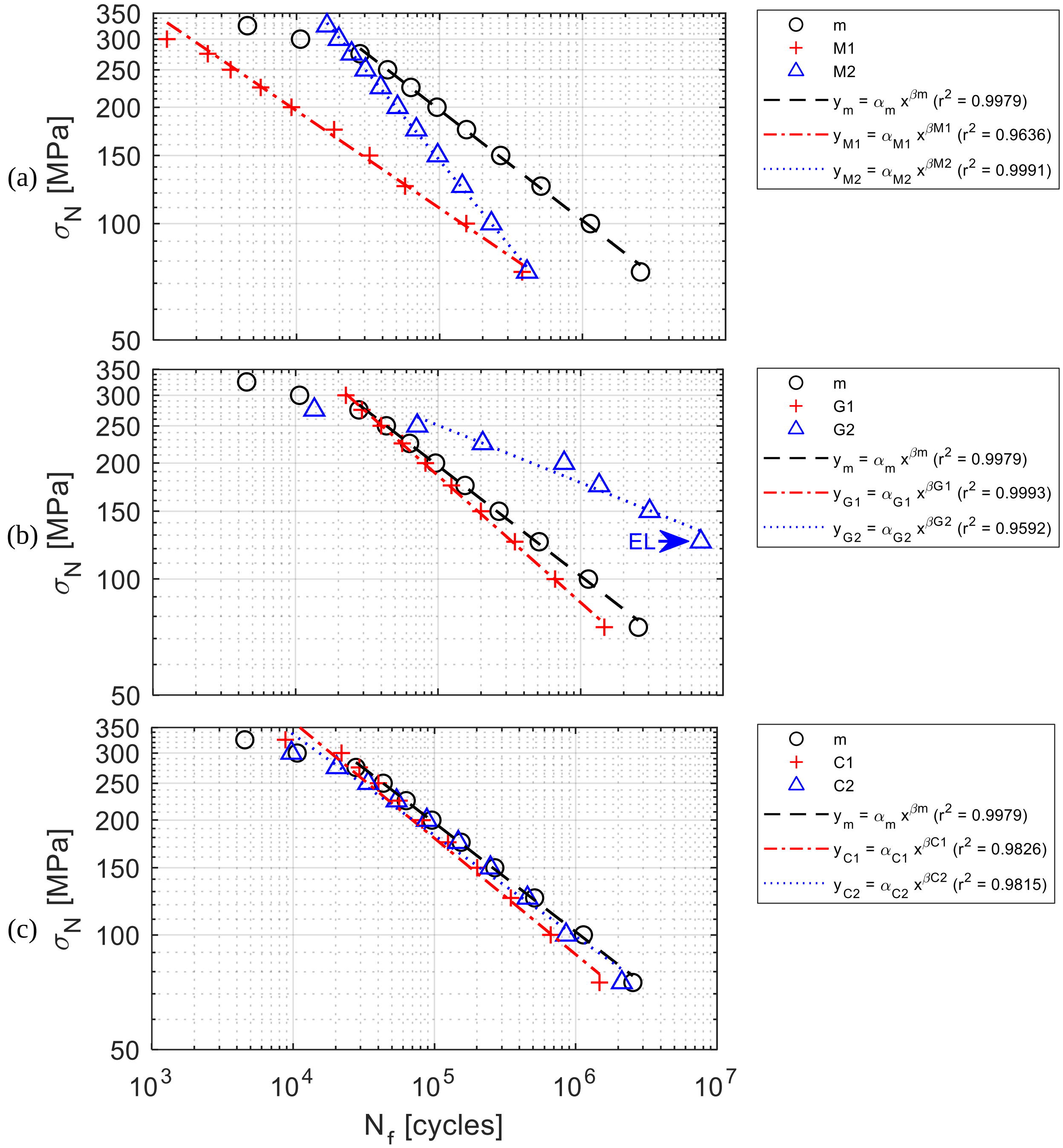

Figure 3: The influence of (a) material (models m, M1, and M2), (b) structure geometry (models m, G1, and G2), and (c) pre-crack shape/dimension (models m, C1, and C2) on the S-N results.

Conclusions

The study supplied simple but reliable three-dimensional modelling and cyclic analysis to simulate crack propagation in welded bridge details subjected to fatigue loading. The approach is based on XFEM technology coupled with LCF approach. S-N curves are provided for a wide range of welded bridge details. The numerical results are compared with both experimental results related to past studies and design curves provided by the regulations. Best-fit S-N curves are developed for enhancing the literature database. The study proves that the developed approach is suitable for various and complex applications, and it can be considered as a reference for similar implementations.

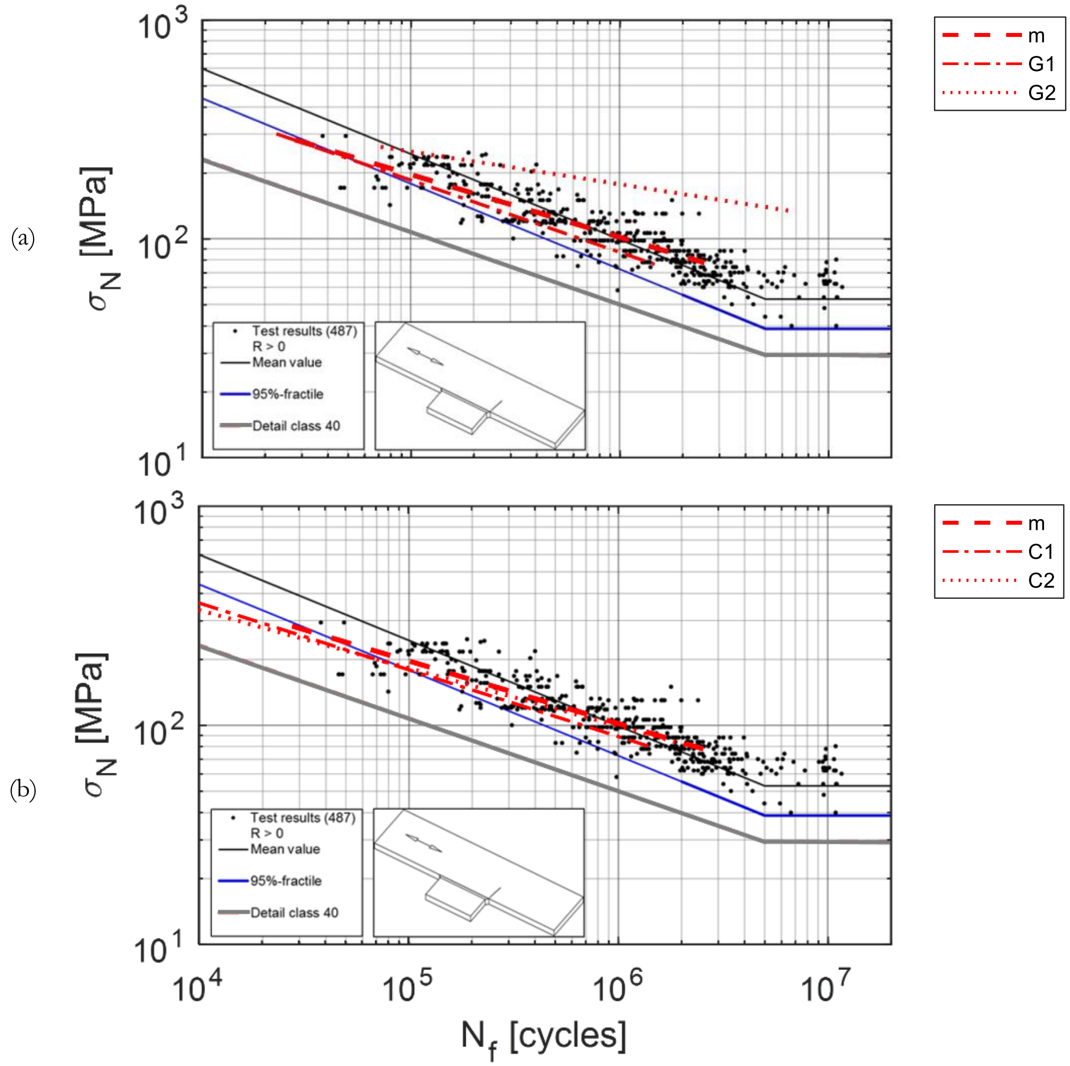

Figure 4: Comparison between the best-fit curves related to the numerical results (dotted and dashed lines) and the experimental results (black dots and thin blue and black lines) reported by Aygül et al. [5] and Aygül [25], together with the C40 detail class curve (thick grey line) provided by Eurocode 3 [5,24]: (a) models m, G1, and G2, and (b) models m, C1, and C2.

Acknowledgments

Computation for the work presented in this paper was supported by the University of Greenwich High Performance Computer resources (https://www.gre.ac.uk/itand-library/hpc). The project was funded by the University of Greenwich under Seedling 2016 and REF 2017/2018 funds.

References

[1] Bergara, A., Dorado, J. I., Martin-Meizoso, A., and Martínez-Esnaola, J. M. (2017). Fatigue crack propagation in complex stress fields: Experiments and numerical simulations using the Extended Finite Element Method (XFEM). International Journal of Fatigue, 103, pp. 112–121. DOI: 1 10.1016/j.ijfatigue.2017.05.026.

[2] D'Angela, D., Ercolino, M., Bellini, C., Di Cocco, V., and Iacoviello, F. (2020). Analysis of acoustic emission entropy for damage assessment of pearlitic ductile cast irons. Material Design & Processing Communications, 12(3), e158. DOI: 10.1002/mdp2.158.

[3] Imam, B., and Chryssanthopoulos, M. K. (2010). A review of metallic bridge failure statistics. IABMAS, Philadelphia, USA.

[4] Wardhana, K., and Hadipriono, F. C. (2003). Analysis of Recent Bridge Failures in the United States. Journal of Performance of Constructed Facilities, 17(3), pp. 144–150. DOI: 10.1061/(ASCE)0887-3828(2003)17:3(144).

[5] Aygül, M., Bokesjö, M., Heshmati, M., and Al-Emrani, M. (2013). A comparative study of different fatigue failure assessments of welded bridge details. International Journal of Fatigue, 49, pp. 62–72. DOI: 10.1016/j.ijfatigue.2012.12.010.

[6] London, T., De Bono, D. M., and Sun, X. (2015). An Evaluation of the Low Cycle Fatigue Analysis Procedure in Abaqus for Crack Propagation: Numerical Benchmarks and Experimental Validation. SIMULIA UK Regional Users Meeting. ID 114881828.

[7] Kim, S.-K., Lee, C.-S., Kim, J.-H., Kim, M.-H., Noh, B.-J., Matsumoto, T., and Lee, J.-M. (2015). Estimation of Fatigue Crack Growth Rate for 7% Nickel Steel under Room and Cryogenic Temperatures Using Damage-Coupled Finite Element Analysis. Metals, 5(2), pp. 603–627. DOI: 10.3390/met5020603.

[8] Zhan, Z., Hu, W., Li, B., Zhang, Y., Meng, Q., and Guan, Z. (2017). Continuum damage mechanics combined with the extended finite element method for the total life prediction of a metallic component. International Journal of Mechanical Sciences, 124–125(C), pp. 48–58. DOI: 10.1016/j.ijmecsci.2017.03.002.

[9] D'Angela, D., and Ercolino, M. (2018). Finite Element Analysis of Fatigue Response of Nickel Steel Compact Tension Samples using ABAQUS. Procedia Structural Integrity, 13, pp. 939–946. DOI: 10.1016/j.prostr.2018.12.176.

[10] Saeedi, M., Azadi, M., Mokhtarishirazabad, M., and Lopez-Crespo, P. (2020). Numerical simulations of carbon/epoxy laminated composites under various loading rates, comparing extended finite element method and cohesive zone modeling. Material Design & Processing Communications, 3(5), e198. DOI: 10.1002/mdp2.198.

[11] Benzaama, A., Mokhtari, M., Benzaama, H., Abdelouahed, E., Tamine, T., Madani, K., Slamen, A., and Ilies, M. (2019). Using XFEM Techniques to Predict the Damage of aluminum 2024T3 notched under tensile load. Frattura ed Integrità Strutturale, 13(50), pp. 184–193. DOI: 10.3221/IGF-ESIS.50.16.

[12] Bhattacharya, S., Singh, I. V., and Mishra, B. K. (2013). Fatigue-life estimation of functionally graded materials using XFEM. Engineering with Computers, 29(4), pp. 427–448. DOI: 10.1007/s00366-012-0261-2.

[13] D'Angela, D., and Ercolino, M. (2021). Fatigue crack growth in metallic components: Numerical modelling and analytical solution. Structural Engineering and Mechanics, 79권(5호), pp. 541–556. DOI: 10.12989/sem.2021.79.5.541.

[14] Giner, E., Díaz-Álvarez, J., Marco, M., and Miguélez, M. H. (2015). Orientation of propagating crack paths emanating from fretting-fatigue contact problems. Frattura ed Integrità Strutturale, 10(35), pp. 285–294. DOI: 10.3221/IGF-ESIS.35.33.

[15] Hedayati E, Vahedi M. (2014)Using Extended Finite Element Method for Computation of the Stress Intensity Factor, Crack Growth Simulation and Predicting Fatigue Crack Growth in a Slant-Cracked Plate of 6061-T651 Aluminum. World Journal of Mechanics 4, pp. 24–30. DOI: 10.4236/wjm.2014.41003.

[16] Talemi, R. H. (2016). Numerical simulation of dynamic brittle fracture of pipeline steel subjected to DWTT using XFEM-based cohesive segment technique. Frattura ed Integrità Strutturale, 10(36), pp. 151–159. DOI: 10.3221/IGF-ESIS.36.1.

[17] Melson, J. H. (2014). Fatigue Crack Growth Analysis with Finite Element Methods and a Monte Carlo Simulation. Degree Thesis. Virginia Polytechnic Institute and State University, Blacksburg, VA.

[18] Simulia. (2016). Abaqus/CAE User's Manual, Version 6.14.

[19] CINDAS/Purdue University (Ed.). (1994). Damage Tolerant Design Handbook. A Compilation of Fracture and Crack-Growth Data for High-Strength Alloys. Lafayette, IN.

[20] De Jesus, A. M. P., Matos, R., Fontoura, B. F. C., Rebelo, C., Simões da Silva, L., and Veljkovic, M. (2012). A comparison of the fatigue behavior between S355 and S690 steel grades. Journal of Constructional Steel Research, 79, pp. 140–150. DOI: /10.1016/j.jcsr.2012.07.021.

[21] Stephens RI, Fuchs HO, editors. Metal fatigue in engineering. 2nd ed. New York: Wiley; 2001.

[22] Kucharski, P., Lesiuk, G., Czapliński, T., Fratczak, R., and Maciejewski, Ł. (2016). Numerical estimation of stress intensity factors and crack propagation in lug connector with existing flaw, 1780(1), 050002. DOI: 10.1063/1.4965949.

[23] Holland, S., Kosel, T., Weaver, R., and Sachse, W. (2000). Determination of plate source, detector separation from one signal. Ultrasonics, 38(1–8), pp. 620–623. DOI: 10.1016/s0041-624x(99)00206-1.

[24] CEN. (2005). EN 1993–1-1. Eurocode 3: Design of steel structures.

[25] Aygül, M. (2012). Fatigue Analysis of Welded Structures Using the Finite Element Method. Degree Thesis. University Of Technology Gothenburg, Sweden.